Electronic Structure and Spectra of Catechol and Alizarin in the Gas Phase and Attached to Titanium

Walter R. Duncan and Oleg V. Prezhdo*

Department of Chemistry, University of Washington, Seattle, Washington 98195-1700

Received: August 13, 2004; In Final Form: September 13, 2004

Ab initio electronic structure calculations elucidate the dramatic differences observed in the electronic spectra of the catechol and alizarin molecules upon binding to titanium. Catechol and alizarin are similar chromophores with analogous electronic spectra in the free state. Binding alizarin to titanium red-shifts the spectrum. The binding of catechol to titanium produces a new optically active transition, at the same time preserving the features of the free catechol spectrum. By examining the details of the calculations, we can rationalize the spectral differences in the catechol and alizarin systems by the positioning of the catechol and alizarin π molecular orbitals relative to the conduction band of TiO_2.

I. Introduction

Electron transfer (ET) at semiconductor surfaces plays a key role in a number of important applications, including photocatalysis, photoelectrolysis, waste processing, quantum confinement devices, and solar cells.[1−5] Solar cells of the Grätzel type are based on transition metal or organic dye molecules that are adsorbed to a highly porous nanocrystalline titanium dioxide.[6,7] The driving force in these cells is the interfacial electron transfer (ET) from the dye to the semiconductor. Upon absorbing light, the dye molecules are excited from their ground state, which is located energetically in the semiconductor band gap, to an excited state that is resonant with the TiO_2 conduction band. The electron is then transferred to the semiconductor on the ultrafast time scale. The relative yields and rates of electron injection, recombination, and decay of the dye-excited state influence the efficiency of the solar cell.[8,9] The competition of charge recombination with the ET pathway lowers the photocurrent. Grätzel cells generally show high photon-to-electron energy conversion yield; low photovoltage, however, remains a limiting factor. Due to electron relaxation, the experimentally observed photovoltage is below the theoretical maximum. Improving the efficiency of the solar devices is possible only when the rates and mechanisms of the competing reactions are known and understood. This in turn requires knowledge of the electronic structure of the dyes both before and after binding to the semiconductor surface.

Numerous experimentalists have investigated the rates and mechanisms of ET in Grätzel type cells.[10−16] Ultrafast laser techniques have shown that electron injection can occur on a femtosecond time scale,[11−14] faster than redistribution of the vibrational energy, in contrast to the traditional ET models.[11] The injection rate has been found to depend on the electronic properties of both the dye and the semiconductor, as well as the distance between the two, as determined by the length of the molecular bridge. Lian and co-workers[13] found that ET between ruthenium-based dyes and TiO_2 occurred on a femtosecond time scale, while ET between the same dyes attached to SnO_2 and ZnO, both of which have a lower density of states (DOS) and, therefore, weaker coupling to the dye, were orders of magnitude slower. A similar effect was observed by changing the length of the bridging units between the dye and the semiconductor: decreasing the donor−acceptor coupling by increasing the dye−semiconductor distance dramatically slowed the ET. By altering the redox potential of dyes attached to SnO_2, Lian et al. were able to affect a range of electron transfer times, while the same dyes attached to TiO_2 all had an electron injection time of less than 100 fs.[13] These and other experimental data clearly point to a complex dependence of the ET rates and mechanisms on the electronic structure of the bound dyes.

Theoretical studies of the dye-sensitized semiconductor systems have focused on chromophore−semiconductor binding,[17−20] electronic structure and spectra of the free and bound chromophore,[21−26] and direct simulation of the electron injection dynamics.[27−33]

Investigations into the dye−semiconductor binding have been done for a number of different systems.[17−20] Grätzel et al.[19] examined the absorption of formic acid and sodium formate on the stoichiometric anatase TiO_2 (101) surface with density functional theory (DFT), Ojamae's group[18] looked at the absorption of formic acid on ZnO ($10\bar{1}0$) surfaces by ab initio Hartree−Fock and gradient-corrected DFT calculations, and Lunell and co-workers[20] investigated the binding of bi-isonicotinic acid to anatase TiO_2 (101) using periodic INDO techniques. Thurnauer's group studied the binding of catechol to TiO_2 nanoparticles with ab initio molecular orbital theory and DFT.[17] The results indicate that catechol reacts with a Ti═O defect site to form a bidentate structure with two chemical bonds to a surface titanium. This structure is more favorable than the configurations that result from either dissociative or molecular adsorption on the (101) anatase surface. The present study uses this bidentate binding structure.

The electronic structure and spectra of dye−semiconductor systems have been the subject of a number of theoretical studies,[21−26] including several that have focused on ruthenium-based dyes.[21−23] In particular, the Gräztel group[21] performed geometry optimizations of *cis*- and *trans*-(Cl_2)bis(4,4′-dicarboxylic acid-2,2′-bipyridine)ruthenium(II) complexes with DFT and then calculated the electronic spectra by ZINDO/S. They found that the three highest occupied molecular orbitals (HOMO) were formed mostly from the 4d orbitals of Ru, while the lowest unoccupied molecule orbitals (LUMO) were almost entirely localized on two $dcbpyH_2$ ligands. The intense absorption in the visible region was assigned to the HOMO to LUMO transition. This and other calculated transitions matched up well with the experimental spectra. Other groups have studied organic dye systems. Catechol was investigated by Lunell and co-

* Corresponding author. E-mail: prezhdo@u.washington.edu.

10.1021/jp046342z CCC: $30.25
Published on Web 12/04/2004

workers,[26] who performed quantum chemical INDO/S-CI calculations of anatase TiO_2 nanoparticles sensitized by catechol and benzoic acid. The experimental observation that catechol causes a strong shift in the TiO_2 absorption threshold, while benzoic acid does not, was explained by a calculation that indicated that only catechol introduces electronic levels in the TiO_2 band gap.

Another series of theoretical investigations has simulated the electron transfer dynamics between the dye molecular donors and the semiconductor acceptors.[27−33] To interpret their pump−probe experimental data and explain the observed coherent oscillations in the spectroscopic signal, Willig and co-workers[27,28] developed a few-dimensional quantum model of the ultrafast electron injection process. The first real-time atomistic simulations of the interfacial ET were carried out in our group[31] by ab initio nonadiabatic molecular dynamics.[30−33] Later, Batista and co-workers[29] used quantum dynamics calculations of electronic relaxation to look at ET in the catechol/TiO_2-anatase system. Both methods reproduced the experimental data of the ultrafast electron injection. Having used the semiempirical Hückel Hamiltonian and assumed decoupling of the electronic and nuclear dynamics, Batista and co-workers were able to simulate a larger system and follow anisotropic charge diffusion through the TiO_2 crystal. Our ab initio simulations of the coupled electron−nuclear dynamics established the electron injection mechanism that varied at low and high temperatures and identified the nuclear motions promoting the ET.

Theoretical calculations help to illustrate the need for a detailed understanding of the solar-cell mechanisms. One example can be found in the process of dye selection. It has been assumed that a high density of conduction band states is needed for efficient ET from the chromophore to the semiconductor in Grätzel cells. The dye is therefore typically chosen to have an excited state well within the conduction band.[7−13,34−38] Upon injection, energy and voltage are lost by a rapid electron relaxation to the bottom of the conduction band. In a recent study of the alizarin−TiO_2 system,[33] we showed that the electronic injection can occur on an ultrafast time scale from photoexcited states at the edge and even below the conduction band, leading to a larger cell voltage.

In elucidating the effect of binding to TiO_2 on the electronic structure and photoexcitation spectra of the electron-donating dyes, it is particularly instructive to compare the alizarin and catechol chromophores that have been recently studied experimentally, both in the free state and bound to titanium. The chromophores, shown in Figure 1, are structurally similar, but behave in remarkably different fashions upon binding. Alizarin has a low-energy band and a prominent high-energy peak that are both red-shifted after binding to a TiO_2 surface.[12] Catechol also has a low-energy band and a stronger high-energy peak. However, in contrast to alizarin, binding catechol to titanium, regardless of whether it is a TiO_2 surface or a single Ti atom in solution, does not red-shift the peaks, but instead creates a new lower energy band.[39] The origin of the spectral changes observed with the alizarin and catechol systems is investigated below with three ab initio quantum chemical techniques, including configuration interaction singles and time-dependent DFT with hybrid and pure DFT functionals.

II. Methods

The electronic structure and spectra of the catechol and alizarin molecules that are in the free state and bound to titanium are investigated using three ab initio quantum chemical approaches. The chromophore spectra predicted by all three approaches have similar features and show similar changes due to binding, but they are shifted with respect to each other in energy. The first technique, configuration interaction singles (CIS), is a wave function-based method in which the excited state is described by a superposition of single-excitation Slater determinants composed of Hartree−Fock (HF) orbitals.[40] CIS is one of the basic approaches for describing excited states and is used here to provide a comparison with the electronic structure and spectra predicted by the two density functional theory (DFT) approaches.

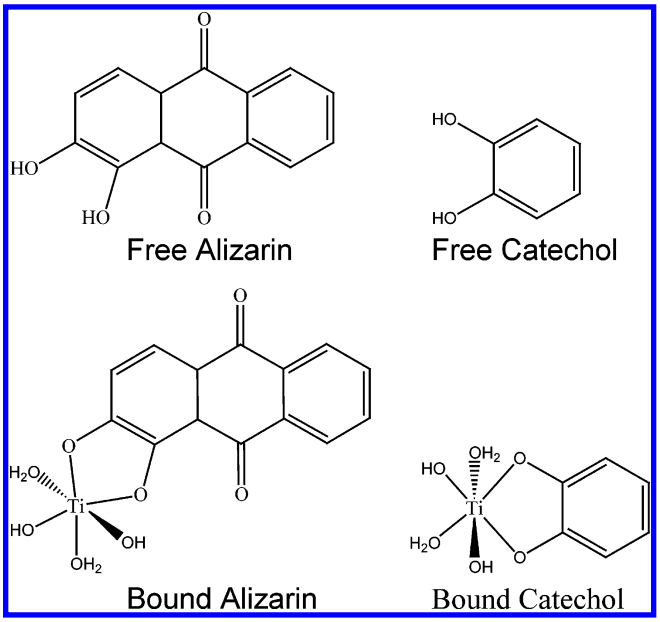

Figure 1. Chemical structure of alizarin and catechol in the free state and bound to titanium, as expected for a neutral species in solution.

Time-dependent DFT (TDDFT) methods provide an improved treatment of the electron correlation effects relative to CIS and, as a result, show better agreement with the experimental spectra. The TDDFT approaches are similar to CIS in implementation,[41] but differ conceptually. The main purpose of the Kohn−Sham molecular orbitals (MOs) of DFT is to represent the one-electron density. In contrast to Kohn−Sham MOs, HF orbitals have well-defined chemical interpretations: frontier orbitals are used to describe chemical reactivity, and orbital energies are related to excitation energies via Koopman's theorem. The simple HF ground state Hamiltonian used in CIS is replaced in TDDFT by sophisticated DFT functionals that take electron correlation into account. The Becke three-parameter-Lee−Yang−Parr (B3LYP) hybrid-DFT exchange−correlation functional[42] and the Perdew−Wang (PW91) exchange−correlation functional[43] are used in the present study. B3LYP has an empirically determined contribution (∼20%) of the nonlocal HF exchange term and, typically, shows excellent agreement with experiment. PW91 is a pure DFT functional that depends only on the local one-electron density and its gradient. Pure DFT methods have the advantage of working well with plane wave basis sets, which are especially suited for the treatment of extended systems, such as the TiO_2-surface-bound alizarin and catechol.[29,33] The calculations reported here are performed with the Gaussian 98 software package using the 6-31g** basis.[44]

We have compared the results of the quantum chemical calculations with the experimental spectra of the free alizarin and catechol chromophores, alizarin and catechol molecules bound to the TiO_2 surface, and catechol bound to a single Ti atom in solution.[12,39] While optical excitations of bulk TiO_2 obscure some spectral features seen with catechol in solution,

TABLE 1: Mulliken Charges on the Bound Catechol and Alizarin Chromophores (Figure 1) in the Ground and First Excited Electronic States

		CIS	B3LYP	PW91
alizarin	ground	−1.21	−0.939	−0.868
	excited	−1.24		
catechol	ground	−1.14	−0.820	−0.740
	excited	−0.70		

the low-energy parts of the spectra are very similar,[39] indicating that the low-energy optical transitions in the catechol−TiO_2 system are localized on the surface. The same can be expected of the alizarin−TiO_2 system. The electronic structure calculations for the alizarin chromophore bound to an extended periodic system representing the TiO_2 surface[33] indeed indicate that the vast majority of the photoexcited orbital is localized on the chromophore, with only a small amount extending onto the Ti ion to which the alizarin is attached. Justified by the reasons discussed above, the spectra of the bound chromophores are studied with a single Ti atom and a set of water and hydroxyl ligands, as would be expected for a neutral complex in solution. The chemical structures of the free and bound alizarin and catechol chromophores used in the calculations are shown in Figure 1. The Mulliken charges localized on the chromophore fragments of the combined chromophore−titanium systems are computed for the ground and excited states and presented in Table 1.

The electronic spectra produced by the CIS and TDDFT ab initio electronic structure calculations constitute a set of lines specified by excitation energies and oscillator strengths that determine excitation intensities. The experimental electronic spectra are broadened due to vibronic substructure as well as homogeneous and inhomogeneous broadening.[45] The widths of the experimental bands of catechol bound to Ti^{4+} in solution are additionally increased by interaction and splitting of the bands of two or three catechols bound to the same Ti ion. To represent the broadening and to facilitate comparison of the calculated data with the experimental spectra, each calculated electronic excitation is assigned a Gaussian with the area proportional to the oscillator strength of that excitation. A single width parameter is chosen for all Gaussians in a given spectrum. For comparison with experiment, the calculated spectra shown in Figures 2 and 5 are shifted in energy. The shifts are minor for the TDDFT data, which show good agreement with the experiment. CIS overestimates the excitation energies and requires significant shifts, as follows. For free alizarin: CIS ($-16\,600$ cm^{-1}); B3LYP (-2000 cm^{-1}); PW91 (2000 cm^{-1}), note the positive sign for PW91, which slightly underestimated the excitation energies of free alizarin. Bound alizarin: CIS ($-19\,750$ cm^{-1}); B3LYP (-4400 cm^{-1}); PW91 (0 cm^{-1}). Free catechol: CIS ($-12\,500$ cm^{-1}); B3LYP (-4000 cm^{-1}); PW91 (-1600 cm^{-1}). Bound catechol: CIS ($-14\,000$ cm^{-1}); B3LYP (-4000 cm^{-1}); PW91 (-2000 cm^{-1}). Thus, each calculated spectrum presented in the figures contains two adjustable parameters, the energy shift and the Gaussian width, both determined by the best fit to the experimental spectrum. The energy shift and Gaussian width are the same for all transitions in a given spectrum. The original theoretical data are presented in Tables 2 and 3. Note that the energy shifts that are needed to match the theoretical and experimental data are smallest with the PW91 density functional, which was used in the nonadiabatic

TABLE 2: Excitation Wavelength and Detailed Orbital Origin of the Six Lowest Energy Optically Active Excitations in Free and Bound Alizarin, as Computed by the Three ab Initio Approaches, with the Excitation Oscillator Strengths Given in Parentheses

	no.	calculated	experimental	wave function
			Free Alizarin	
CIS	1	252(0.29)	431	$0.63\|H \rightarrow L\rangle$
	2	231(0.091)	431/325	$0.60\|H\text{-}1 \rightarrow L\rangle$
	3	221(0.11)	325	$0.46\|H\text{-}3 \rightarrow L\rangle+0.29\|H \rightarrow L+1\rangle+0.24\|H\text{-}1 \rightarrow L+1\rangle$
	4	183(0.37)	<300	$0.41\|H \rightarrow L+1\rangle-0.24\|H\text{-}1 \rightarrow L+1\rangle$
	5	180(1.0)	<300	$0.53\|H\text{-}2 \rightarrow L+1\rangle-0.27\|H\text{-}1 \rightarrow L\rangle$
	6	171(0.83)	<300	$0.43\|H\text{-}3 \rightarrow L\rangle-0.37\|H\text{-}1 \rightarrow L+1\rangle$
TDDFT	1	388(0.12)	431	$0.65\|H \rightarrow L\rangle$
(B3LYP)	2	318(0.049)	325	$0.52\ \|H\text{-}3 \rightarrow L\rangle-0.40\|H\text{-}4 \rightarrow L\rangle$
	3	276(0.13)	<300	$0.62\|H\text{-}5 \rightarrow L\rangle$
	4	246(0.090)	<300	$0.50\|H \rightarrow L+2\rangle-0.31\|H\text{-}4 \rightarrow L+1\rangle-0.28\|H\text{-}3 \rightarrow L+1\rangle$
	5	273(0.069)	<300	$0.51\|H\text{-}4 \rightarrow L+1\rangle-0.29\|H\text{-}3 \rightarrow L+1\rangle$
	6	235(0.26)	<300	$0.48\|H\text{-}3 \rightarrow L+1\rangle-0.34\|H\text{-}5 \rightarrow L+1\rangle$
TDDFT	1	465(0.087)	431	$0.63\|H\text{-}1 \rightarrow L\rangle$
(PW91)	2	312(0.071)	325/	$0.56\|H\text{-}5 \rightarrow L\rangle$
	3	279(0.038)	<300	$0.50\|H\text{-}1 \rightarrow L+2\rangle-0.35\|H\text{-}3 \rightarrow L+1\rangle$
	4	262(0.36)	<300	$0.44\|H\text{-}3 \rightarrow L+1\rangle-0.30\|H\text{-}5 \rightarrow L+1\rangle+0.26\|H\text{-}1 \rightarrow L+2\rangle$
	5	258(0.037)	<300	$0.50\|H\text{-}5 \rightarrow L+1\rangle+0.28\|H\text{-}1 \rightarrow L+2\rangle-0.27\|H\text{-}3 \rightarrow L+3\rangle$
	6	230(0.13)	<300	$0.42\|H\text{-}4 \rightarrow L+2\rangle+0.30\|H\text{-}5 \rightarrow L+3\rangle-0.24\|H\text{-}4 \rightarrow L+3\rangle$
			Bound Alizarin	
CIS	1	253(0.30)	503	$0.62\|H \rightarrow L\rangle$
	2	240(0.041)	503	$0.48\|H\text{-}1 \rightarrow L\rangle+0.31\|H \rightarrow L+2\rangle$
	3	221(0.084)	<350	$0.57\|H\text{-}2 \rightarrow L\rangle$
	4	219(0.042)	<350	$0.40\|H\text{-}3 \rightarrow L\rangle+0.27\|H \rightarrow L+2\rangle$
	5	204(0.089)	<350	$-0.40\|H \rightarrow L+5\rangle+0.26\|H \rightarrow L+7\rangle$
	6	198(0.11)	<350	$-0.29\|H \rightarrow L+6\rangle+0.27\|H \rightarrow L+7\rangle$
TDDFT	1	411(0.10)	503	$0.55\|H \rightarrow L\rangle-0.37\|H \rightarrow L+1\rangle$
(B3LYP)	2	391(0.044)	503	$0.55\|H \rightarrow L+1\rangle+0.34\|H \rightarrow L\rangle$
	3	301(0.046)	<350	$0.65\|H\text{-}4 \rightarrow L\rangle$
	4	293(0.11)	<350	$0.52\|H\text{-}2 \rightarrow L+1\rangle-0.26\|H\text{-}1 \rightarrow L+2\rangle+0.24\|H \rightarrow L+4\rangle$
	5	279(0.10)	<350	$0.57\|H\text{-}1 \rightarrow L+2\rangle$
	6	273(0.079)	<350	$-0.52\|H\text{-}2 \rightarrow L+2\rangle+0.34\|H\text{-}5 \rightarrow L\rangle$
TDDFT	1	497(0.073)	503	$0.55\|H \rightarrow L\rangle-0.24\|H\text{-}1 \rightarrow L\rangle-0.24\|H \rightarrow L+1\rangle$
(PW91)	2	352(0.044)	<350	$0.56\|H \rightarrow L+4\rangle$
	3	340(0.11)	<350	$0.47\|H\text{-}3 \rightarrow L+1\rangle-0.26\|H\text{-}2 \rightarrow L+3\rangle$
	4	308(0.052)	<350	$0.45\|H\text{-}5 \rightarrow L\rangle+0.34\|H\text{-}5 \rightarrow L+1\rangle$
	5	280(0.052)	<350	$0.47\|H\text{-}3 \rightarrow L+4\rangle-0.25\|H\text{-}4 \rightarrow L+3\rangle$
	6	270(0.099)	<350	$0.41\|H\text{-}9 \rightarrow L\rangle+0.36\|H \rightarrow L+6\rangle$

TABLE 3: Excitation Wavelength and Detailed Orbital Origin of the Six Lowest Energy Optically Active Excitations in Free and Bound Catechol, as Computed by the Three ab Initio Approaches, with the Excitation Oscillator Strengths Given in Parentheses

	no.	calculated	experimental	wave function
			Free Catechol	
CIS	1	204(0.058)	275	$0.59\|H \rightarrow L\rangle + 0.37\|H\text{-}1 \rightarrow L+1\rangle$
	2	148(1.1)	210/<200	$0.50\|H\text{-}1 \rightarrow L\rangle + 0.45\|H \rightarrow L+1\rangle$
	3	147(1.1)	210/<200	$0.58\|H\text{-}1 \rightarrow L+1\rangle - 0.35\|H \rightarrow L\rangle$
	4	99(0.043)	<200	$-0.42\|H\text{-}7 \rightarrow L+2\rangle + 0.41\|H\text{-}4 \rightarrow L+2\rangle$
	5	92(0.047)	<200	$0.55\|H\text{-}5 \rightarrow L\rangle$
	6	90(0.055)	<200	$0.40\|H\text{-}4 \rightarrow L+3\rangle - 0.37\|H\text{-}3 \rightarrow L+3\rangle$
TDDFT	1	245(0.042)	275	$0.60\|H \rightarrow L\rangle - 0.36\|H\text{-}1 \rightarrow L+1\rangle$
(B3LYP)	2	211(0.040)	210	$0.55\|H \rightarrow L+1\rangle + 0.35\|H\text{-}1 \rightarrow L\rangle$
	3	183(0.36)	<200	$0.51\|H\text{-}1 \rightarrow L\rangle - 0.29\|H \rightarrow L+1\rangle$
	4	178(0.51)	<200	$0.54\|H\text{-}1 \rightarrow L+1\rangle + 0.24\|H \rightarrow L\rangle$
	5	149(0.085)	<200	$0.65\|H\text{-}2 \rightarrow L\rangle$
	6	135(0.12)	<200	$0.68\|H\text{-}5 \rightarrow L\rangle$
TDDFT	1	260(0.037)	275	$0.59\|H \rightarrow L\rangle - 0.34\|H\text{-}1 \rightarrow L+1\rangle$
(PW91)	2	222(0.051)	210	$0.56\|H \rightarrow L+1\rangle + 0.29\|H\text{-}1 \rightarrow L\rangle$
	3	195(0.22)	<200	$0.52\|H\text{-}1 \rightarrow L\rangle - 0.24\|H \rightarrow L+1\rangle$
	4	186(0.40)	<200	$0.52\|H\text{-}1 \rightarrow L+1\rangle - 0.24\|H\text{-}2 \rightarrow L\rangle$
	5	161(0.15)	<200	$0.59\|H\text{-}2 \rightarrow L\rangle$
	6	149(0.19)	<200	$0.65\|H\text{-}5 \rightarrow L\rangle$
			Bound Catechol	
CIS	1	266(0.085)	380	$0.51\|H \rightarrow L+2\rangle + 0.43\|H \rightarrow L+4\rangle$
	2	197(0.19)	272	$-0.36\|H\text{-}1 \rightarrow L\rangle + 0.33\|H \rightarrow L+3\rangle + 0.30\|H \rightarrow L+8\rangle$
	3	191(0.088)	272	$0.34\|H \rightarrow L+3\rangle - 0.30\|H \rightarrow L+8\rangle$
	4	157(0.079)	<200	$0.28\|H\text{-}11 \rightarrow L+4\rangle + 0.24\|H\text{-}11 \rightarrow L+3\rangle$
	5	156(0.056)	<200	$-0.31\|H\text{-}6 \rightarrow L+3\rangle + 0.30\|H\text{-}6 \rightarrow L+2\rangle$
	6	154(0.044)	<200	$0.27\|H\text{-}7 \rightarrow L\rangle + 0.24\|H\text{-}6 \rightarrow L\rangle$
TDDFT	1	390(0.15)	380	$-0.52\|H\text{-}1 \rightarrow L\rangle - 0.24\|H \rightarrow L+2\rangle$
(B3LYP)	2	244(0.055)	272	$0.41\ \|H\text{-}5 \rightarrow L+2\rangle + 0.29\|H\text{-}9 \rightarrow L\rangle - 0.28\|H \rightarrow L+6\rangle$
	3	205(0.042)	<200	$0.65\|H\text{-}4 \rightarrow L+3\rangle$
	4	200(0.039)	<200	$0.63\|H\text{-}53 \rightarrow L+3\rangle$
	5	185(0.14)	<200	$0.47\|H\text{-}1 \rightarrow L+6\rangle + 0.29\|H\text{-}10 \rightarrow L+1\rangle$
	6	184(0.039)	<200	$0.42\|H\text{-}7 \rightarrow L+3\rangle - 0.39\|H\text{-}10 \rightarrow L+1\rangle - 0.26\|H\text{-}4 \rightarrow L+4\rangle$
TDDFT	1	436(0.12)	380	$-0.39\|H \rightarrow L+2\rangle - 0.33\|H\text{-}1 \rightarrow L\rangle$
(PW91)	2	255(0.079)	272	$0.47\|H \rightarrow L+6\rangle - 0.27\|H\text{-}1 \rightarrow L+8\rangle - 0.26\|H \rightarrow L+5\rangle$
	3	238(0.047)	272	$-0.46\|H\text{-}8 \rightarrow L+1\rangle - 0.25\|H\text{-}7 \rightarrow L+2\rangle$
	4	201(0.11)	<200	$0.42\|H\text{-}3 \rightarrow L+5\rangle + 0.42\|H\text{-}3 \rightarrow L+6\rangle$
	5	195(0.062)	<200	$-0.34\|H\text{-}4 \rightarrow L+5\rangle + 0.34\|H\text{-}1 \rightarrow L+6\rangle$
	6	194(0.086)	<200	$0.55\|H\text{-}7 \rightarrow L+4\rangle$

molecular dynamics simulation of the isonicotinic acid−titanium[30−32] and the alizarin−titanium systems.[33]

III. Results and Discussion

The bonding of the catechol and alizarin molecules to the Ti atom occurs by interaction between electron pairs on the hydroxyl oxygens and the d orbitals of the Ti atom. The Mulliken charges localized on the chromophore ligands and computed for the ground and excited states of the combined chromophore−titanium systems are reported in Table 1. A slightly smaller chromophore charge is observed for catechol compared to alizarin. While the ground state charges on the alizarin and catechol chromophores are quite similar, the charges in the first excited state are noticeably different, as elucidated below.

We first analyze the excitation spectra of the alizarin molecule in its free state and bound to titanium. Although alizarin is a larger molecule with a slightly more complicated electronic structure than catechol, its experimental spectrum shows only a slight shift upon binding to titanium, while the spectrum of the bound catechol shows a new transition that does not exist in the free catechol. The experimental spectra for free alizarin (left) and alizarin bound to the TiO_2 surface (right) are shown in Figure 2 by dark circles that form a nearly continuous thick line. The lowest energy band in the electronic spectrum of free alizarin (solid arrow) is centered at 431 nm. The next band is much stronger and is centered below 250 nm with a shoulder at approximately 325 nm (dotted arrow). Both bands are red shifted upon binding to titanium, with the lowest energy band shifted by approximately 70 nm.

The theoretical spectrum (dark gray line) is computed as the sum of the Gaussians that represent individual electronic excitations (light gray lines). In both free and bound alizarin the lowest energy band is dominated by a single electronic excitation, with minor contributions from several others that are less optically active. The broad second band is formed by a large number of excitations. The agreement between the experimental and theoretical spectra is quite good, although the CIS data had to be significantly shifted to lower energies, as discussed in the Methods section.

The orbital origins of the six lowest energy, optically active excitations in the free and bound alizarin are detailed in Table 2, which lists the experimental and calculated excitation wavelengths, together with a few dominant orbital transitions for each electronic excitation. Due to spatial constraints, only electronic excitations with oscillator strengths above 0.0345 are included in the tables, and only orbital transitions with coefficients whose magnitudes are 0.24 or larger are shown.

The excitation wavelengths are reported in the tables exactly as calculated by the CIS, TDDFT(B3LYP), and TDDFT(PW91) approaches, without the shifting used to match the experimental spectra in Figure 2. Clearly, PW91 and B3LYP are in best agreement with the experimental results. Somewhat unexpectedly, PW91 agrees with the data better than does B3LYP, nearly exactly matching the experimentally measured lowest excitation energy of the bound alizarin. Note that the nonadiabatic molecular dynamics simulations of the ultrafast electron injection from alizarin to the TiO_2 surface that were performed in our group used the PW91 density functional.[33] CIS significantly underestimates the excitation wavelengths, as expected. The

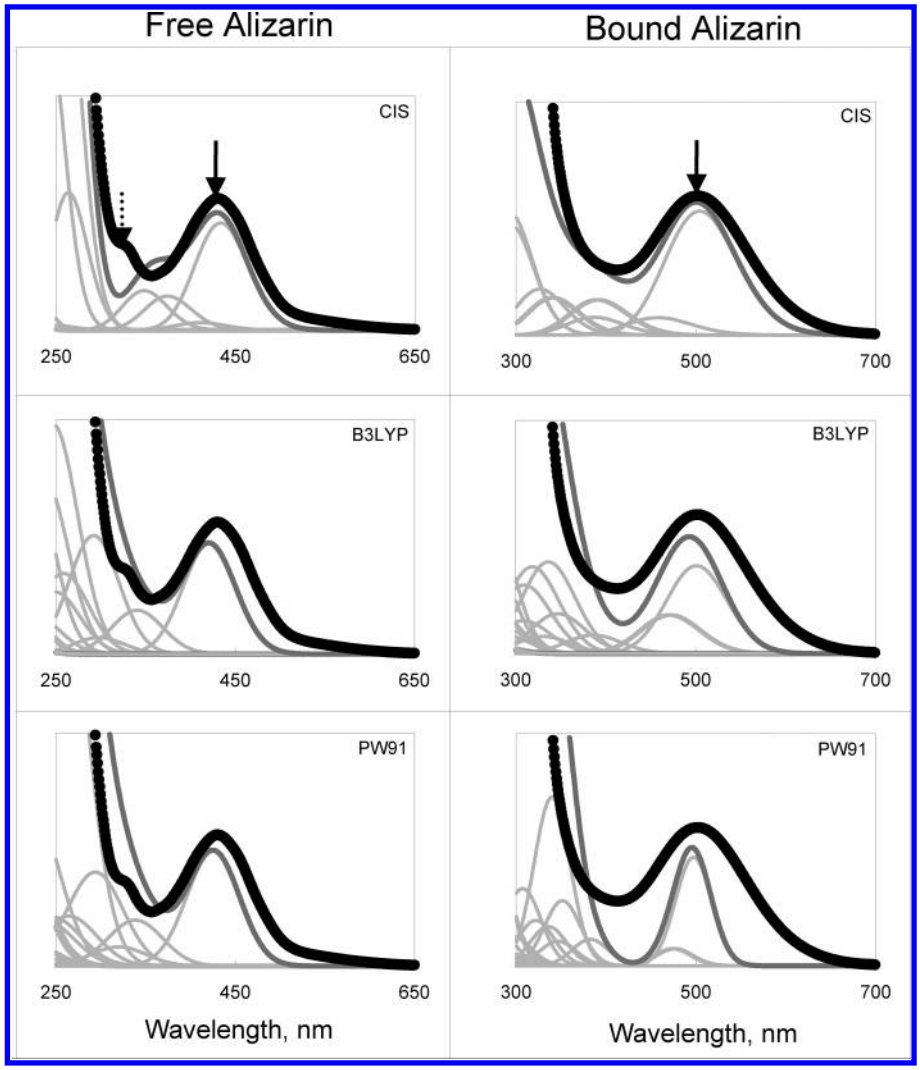

Figure 2. Spectra of free and bound alizarin measured experimentally[12] (black dots merging into a thick black line) and calculated theoretically (gray lines) by several ab initio approaches, as indicated in the plots and detailed in the main text. The left column corresponds to free alizarin, while the right column represents bound alizarin. The binding to titanium red-shifts the main transition (solid arrows) by ~70 nm.

lowest energy photoexcitation of the free alizarin at 431 nm is dominated by the transition between the highest occupied molecular orbital (HOMO) and the lowest unoccupied molecular orbital (LUMO), except for the case of PW91, where it is between the (HOMO−1) and the LUMO. The PW91 (HOMO−1) matches the CIS and the B3LYP HOMO, and therefore all three techniques describe the same transition. The HOMO−LUMO transition also makes the largest contribution to the lowest energy photoexcitation of the bound alizarin at 503 nm, although noticeable contributions from other orbital transitions are observed, in particular with the DFT calculations. All the bound HOMOs and LUMOs match each other extremely well, except the PW91 HOMO. It appears that the HOMO from the other two techniques is spread over the PW91 HOMO and (HOMO−1). This helps to explain the large contribution from both the HOMO−LUMO and (HOMO−1)−LUMO transitions (Table 2). The similarity between the free and bound cases (Figure 2) is due to the fact that the first excited state of the alizarin molecule lies below the Ti d orbitals such that binding alizarin to titanium leads to only a minor mixing of the alizarin π-HOMO and π^*-LUMO with the Ti. In bulk TiO_2 the mixing of the Ti d orbitals leads to a conduction band that puts the alizarin excited state at the very edge of the band.

Figure 3 shows the MO energy diagrams of the free and bound alizarin. The energy scale used in the figure is the same for all three methods, emphasizing that CIS overestimates the excitation energies relative to TDDFT(B3LYP) and TDDFT-(PW91), both of which agree well with experiment (Table 2). The orbital excitations shown by the arrows in Figure 3 correspond to the optical transitions marked by the arrows in the spectra in Figure 2. The solid arrow depicts the lowest energy band dominated by the HOMO−LUMO excitation. The dotted arrow indicates the shoulder of the second band in the free alizarin spectrum (Figure 2). Binding to titanium, and the subsequent redistribution of electron density, slightly shifts the orbital energies and decreases the gap between the occupied and vacant orbitals.

Figure 4 shows the HOMO and LUMO images of the free and bound alizarin. The orbitals are taken from the HF/CIS calculation. The corresponding DFT orbitals look similar to the HF orbitals. The HOMO of free alizarin is a π orbital localized toward the hydroxyl end of the molecule. The lone electron pairs of the hydroxyl and quinone oxygens contribute to the alizarin HOMO. The free alizarin LUMO is evenly localized over the whole molecule, including the oxygen atoms. The hydroxyl groups by which alizarin attaches to TiO_2 contribute to both HOMO and LUMO, creating favorable conditions for interaction with the titanium. Since the energies of the Ti d orbitals are beyond the range of the alizarin HOMO and LUMO, the HOMO and LUMO of the combined alizarin−titanium

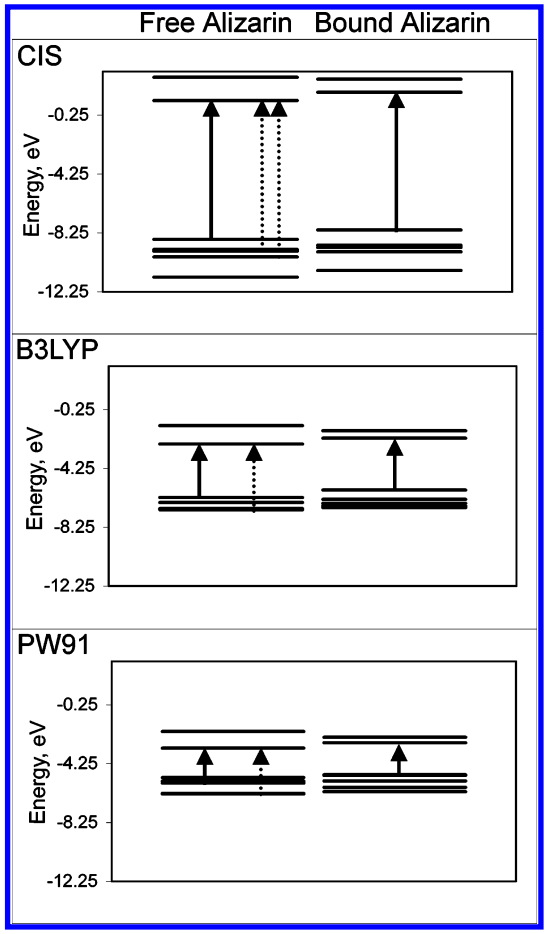

Figure 3. Theoretically determined molecular orbital energies and transitions in free (left) and bound (right) alizarin. The solid arrows correspond to the transition at 431 nm for free alizarin and 503 nm for bound alizarin, cf. Figure 2. Both transitions are dominated by the HOMO to LUMO excitation (see Table 1 for detailed analysis). The dotted arrows indicate the free alizarin transition at 325 nm. CIS significantly overestimates the excitation energy for both free and bound alizarin. The DFT-based approaches are in good agreement with experiment for free alizarin, and PW91 exactly matches the experimental excitation energy for bound alizarin.

system are nearly the same as those of the free alizarin. This is consistent with the fact that the optical excitation energies and localizations are similar in the free and bound alizarin (Figure 2 and Table 2). Since the HOMO−LUMO photoexcitation redistributes little electron density between alizarin and titanium, the charge on alizarin remains the same in the ground and excited states (Table 1).

We observe a significantly more interesting and richer optical picture with the catechol system, even though it is smaller and analogous to the alizarin system (Figure 1). The experimental spectra are shown in Figure 5 for free (left) and bound (right) catechol by dark circles that form a nearly continuous dark line. The electronic excitations in catechol are higher in energy when compared to alizarin, since catechol is smaller, with a less delocalized π electron system. The lowest excitation in catechol occurs at 275 nm (solid arrow), compared to 431 nm in alizarin. As in alizarin, the lowest optical band in free catechol is dominated by a single electronic excitation, primarily of the HOMO−LUMO origin (Table 3). The second optical band is stronger than the first, comprises many excitations, and is centered below 200 nm with a shoulder at approximately 210 nm. The shoulder is highlighted by a dotted arrow in Figure 5.

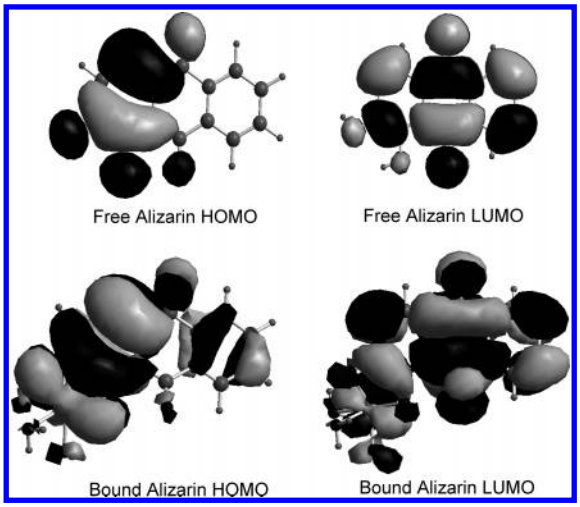

Figure 4. Molecular orbitals involved in the excitations of free (top) and bound (bottom) alizarin at 431 and 503 nm, respectively, marked by the solid arrows in Figure 2. In each case the excitation is dominated by a HOMO to LUMO transition. Apart from a small contribution from the titanium, the bound alizarin orbitals are nearly identical to those of the free alizarin. The Hartree−Fock orbitals are similar to the Kohn−Sham orbitals.

Strong absorption from bulk TiO_2 at 350 nm and below obscures the excitations of the surface-bound catechol. The details of the bound catechol spectra are more pronounced in solution, with catechol attached to a single Ti atom. This experimental spectrum is shown in Figure 5. Binding to titanium has an entirely different effect on catechol than on alizarin. While the overall features of the free alizarin spectrum remain the same, and the entire spectrum undergoes a slight red-shift (Figure 2), a new optical band appears at low energy in the bound catechol spectrum, and the bands from the free catechol spectrum remain unshifted (Figure 5). The new broad band that peaks at 380 nm is primarily due to a single excited state that results from the direct photoexcitation-induced electron transfer from the π-HOMO of catechol to the d orbitals of Ti. 44% of an electron moves from catechol to titanium upon photoexcitation, as indicated by Table 1.

The agreement between the experimental and theoretical spectra in Figure 5 is quite good, but, as with alizarin, the CIS data have to be significantly shifted to lower energies. The CIS method also does not reproduce the shoulder on the large peak (dotted arrow), whereas both TDDFT methods do predict a shoulder. The large width of the new low-energy band in the bound catechol spectrum observed in the experimental data is most likely due to coupling and splitting of the bands of two or three catechol molecules that are bound to the same Ti atom in solution. The calculations were performed for a single catechol (Figure 1).

The orbital origins of the six lowest energy, optically active excitations in free and bound catechol are detailed in Table 3, which lists the experimental and calculated excitation wavelengths, together with a few dominant orbital transitions for each electronic excitation. As with alizarin, the cutoff on the oscillator strength of the excitations presented in the Table is 0.0345. The cutoff on the magnitude of the orbital transition coefficients is 0.24. The excitation wavelengths are reported in the tables exactly as calculated by the CIS, TDDFT(B3LYP), and TDDFT-(PW91) approaches, without the shifting used to match the experimental spectra in Figure 5. Whereas the excitations that make up the low-energy band in free alizarin and the corresponding band in bound alizarin are dominated by the HOMO−

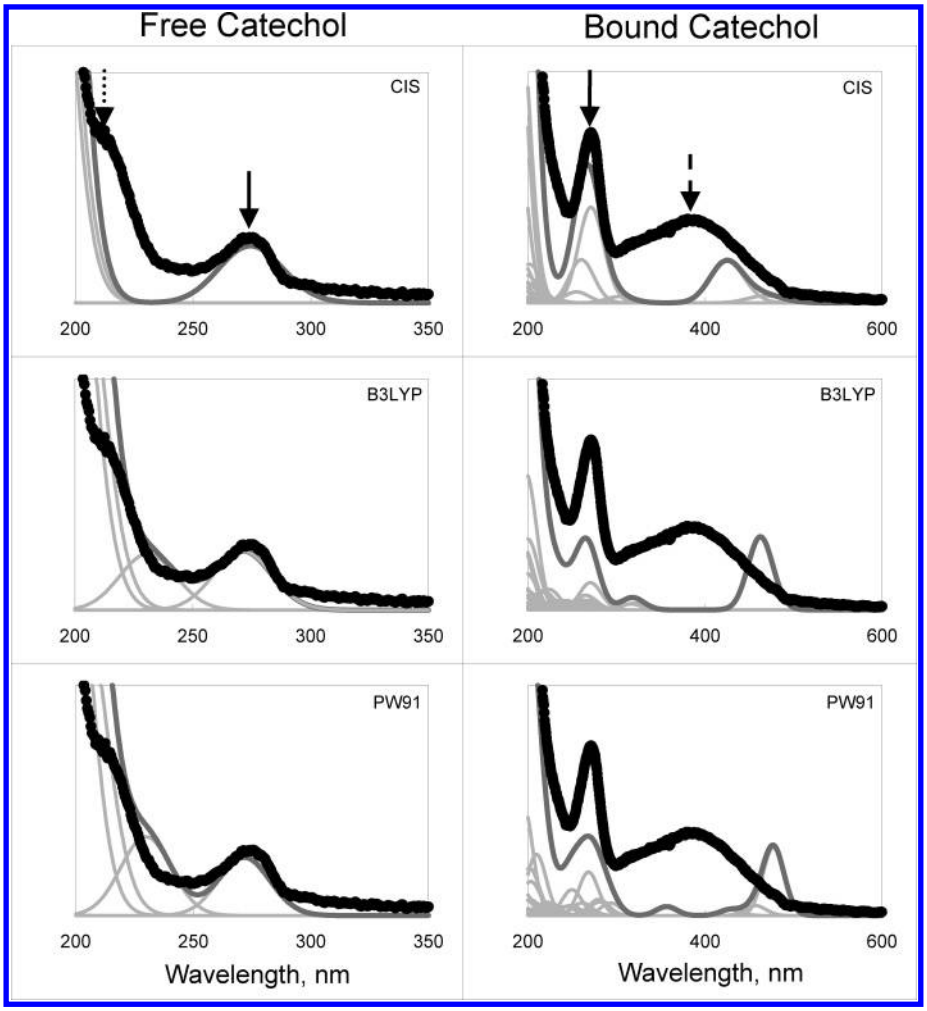

Figure 5. Spectra of free and bound catechol measured experimentally[39] (black dots merging into a thick black line) and calculated theoretically (gray lines) by several ab initio approaches, as indicated in the plots and detailed in the main text. The left column corresponds to free catechol, while the right column represents bound catechol. In contrast to alizarin, Figure 2, binding to titanium creates a new absorption band in catechol (dashed arrow), leaving the wavelength of the original transition unchanged (solid arrow).

LUMO transitions, this is not the case with catechol. While the HOMO−LUMO transition dominates the lowest excitation in free catechol at 275 nm, in bound catechol it makes no contribution to the corresponding excitation at 272 nm. The difference in the excitations is due to a difference in the ordering of the orbitals. The LUMO of free alizarin is very similar to the LUMO of bound alizarin. The LUMO of free catechol, however, corresponds to a higher energy unoccupied molecular orbital in the bound system. The LUMO of bound catechol has the largest contribution from a d electron orbital of the Ti. The ordering of the orbitals in the single titanium complex reflects the positioning of the orbitals in catechol bound to a TiO_2 surface, where the energy of the free catechol LUMO is well inside the conduction band. The new band at 380 nm involves transitions between the catechol HOMO and several low-lying excited orbitals, including the LUMO, which have predominantly titanium character.

Figure 6 shows the energy diagrams for the MOs of the free and bound catechol. As with alizarin (Figure 2), the energy scale is the same for all three methods, showing that CIS overestimates the excitation energies relative to TDDFT(B3LYP) and TDDFT(PW91), which are in good agreement with experiment (Table 3). The orbital transitions shown by the arrows in Figure 6 correspond to the bands marked by the arrows in the spectra in Figure 5. For free catechol, the solid arrow depicts the lowest energy band, dominated by the HOMO−LUMO transition, while the dotted arrow indicates the shoulder of the higher energy band. For bound catechol, the solid arrow indicates the transition between the orbitals that best match the free dye HOMO and LUMO. The dashed arrow depicts the new transition to low-lying Ti d orbitals. The bound catechol orbitals shift upward in energy relative to free catechol, due to the transfer of charge from Ti to catechol upon binding.

Figure 7 shows images of the orbitals involved in the dominant transitions for free and bound catechol. The orbitals are taken from the HF/CIS calculation. For free catechol the DFT orbitals are the same as the ones calculated with HF. For bound catechol the DFT HOMOs match the HF HOMO, and the DFT (LUMO+6) orbitals match the HF (LUMO+8). The bound HOMO and (LUMO+8) orbitals closely resemble the free catechol HOMO and LUMO. The HF (LUMO+2), made predominantly of a d orbital, gives the largest contribution to the new low-energy band at 380 nm in the titanium-bound catechol (Table 3). Our results agree with earlier studies of catechol bound to titanium.[26,29] By performing calculations with a cluster representation of TiO_2 Lunell and co-workers[26] found that the HOMO of catechol attached to a TiO_2 cluster also matches the HOMO of the free dye and that the low-energy band in bound catechol is dominated by an excitation from the HOMO to a TiO_2 orbital.

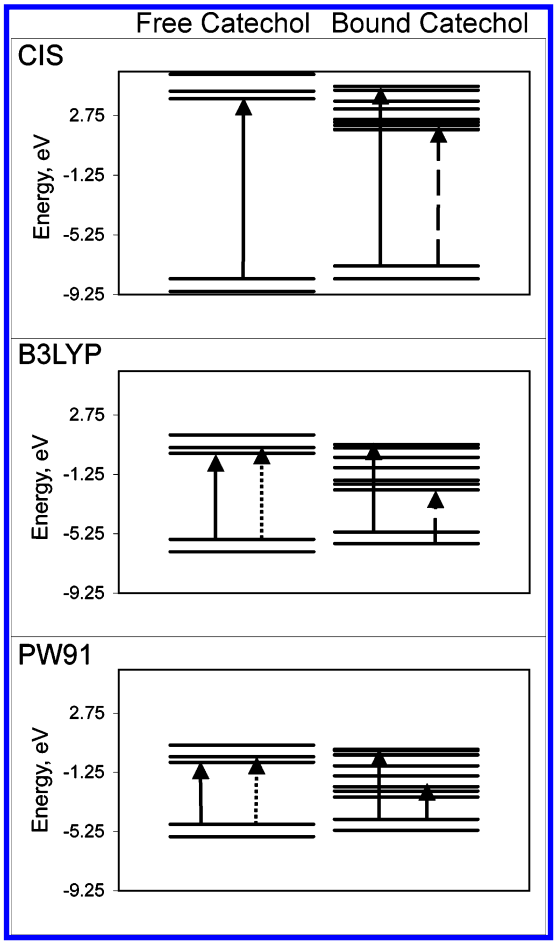

Figure 6. Theoretically determined molecular orbital energies and transitions in free (left) and bound (right) catechol. The solid arrows correspond to the transition at 275 nm for free catechol and 272 nm for bound catechol, cf. Figure 5. The free catechol transition at 275 nm is dominated by a HOMO to LUMO excitation. The d orbitals of titanium lie below the LUMO for free catechol, such that binding to titanium creates a new transition at 380 nm (dashed arrow). The dotted arrows indicate the free catechol transition at 210 nm. CIS significantly overestimates the excitation energy for both free and bound catechol. The DFT-based approaches are in good agreement with experiment.

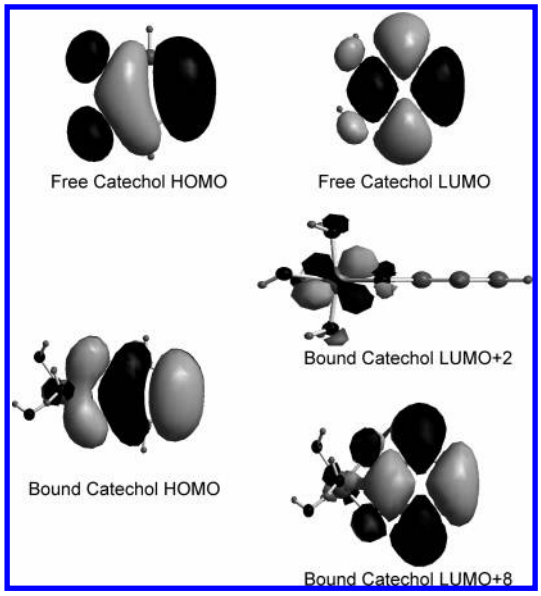

Figure 7. Molecular orbitals involved in the excitations of free (top) and bound (bottom) catechol marked by the solid arrows (275 and 272 nm, respectively) and the dashed arrow (380 nm) in Figures 5 and 6. For free catechol the solid arrow excitation is dominated by a HOMO to LUMO transition. The corresponding excitation in bound catechol is between HOMO and LUMO+8. These orbitals are nearly identical in free and bound catechol. The lowest energy optical excitation in the bound catechol marked by the dashed arrow involves HOMO and LUMO+2, the latter orbital strongly localized on the titanium. The shown Hartree−Fock orbitals are similar to the Kohn−Sham orbitals.

IV. Conclusions

The spectra of the catechol and alizarin molecules in the free state and bound to titanium have been simulated using three different ab initio quantum chemical techniques: CIS, TDDFT-(B3LYP), and TDDFT(PW91). All three calculation methods accurately predict the shape of the experimental free spectra and the effect of binding to titanium, with the TDDFT methods more accurately predicting the excitation energies.

Although catechol and alizarin are very similar molecules with analogous electronic spectra in the free state, they show stark differences upon binding to titanium. The alizarin spectrum is red-shifted upon binding, but retains its shape. Binding catechol to titanium, on the other hand, causes very little shifting of the spectrum, but does produce a new low-energy band. The calculations show that the low-energy bands in both free alizarin and free catechol are due to single electronic excitations that are dominated by orbital transitions between the HOMO and LUMO. The same can be said of bound alizarin, where the calculations show that the bound HOMO and LUMO match the orbitals of the free chromophore, with only small contributions from the Ti. In bound catechol, however, the LUMO is mostly localized on the titanium, and the free catechol LUMO becomes a higher energy orbital. The new low-energy band observed in the bound catechol spectrum is dominated by transitions from the dye-localized HOMO to several titanium-localized unoccupied orbitals. The theoretical results show that alizarin and catechol exhibit such different behavior upon binding to titanium because of the positioning of their π molecular orbitals relative to the d orbitals of the titanium that form the conduction band of TiO_2. The superiority of the PW91 technique, particularly to the CIS method, in reproducing the experimental spectra supports the choice of this method to describe the ultrafast ET dynamics in Grätzel cells.[30−33]

The presented theoretical study of the electronic structure of the alizarin and catechol molecules bound to titanium demonstrates three types of photoexcited states: *first*, the chromophore excited state that is near the edge of the TiO_2 conduction band, as exemplified by the alizarin system; *second*, the chromophore excited state that is well inside the conduction band, as seen with catechol; *third*, a new state near the band edge that appears because of the direct photoexcitation from the chromophore to the semiconductor, also seen with catechol. The strong chromophore−semiconductor coupling is required for the state of the third type to be optically active. Experimental and theoretical work show that catechol and alizarin both rapidly inject the photoexcited electron into the TiO_2 conduction band.[14,16,29,33] Injection near the bottom of the conduction band is preferred,[33] since electrons injected high in the band rapidly relax to the bottom. Higher voltages are expected with Grätzel cells driven by photoexcitation into the states of the first and third kind.

Acknowledgment. The authors are grateful to Drs. Lian and Wachtveitl for providing the original experimental data. The research was supported by NSF, CAREER Award CHE-0094012. O.V.P. is an Alfred P. Sloan Fellow.

References and Notes

(1) Ferrere, S.; Gregg, B. *J. Phys. Chem. B* **2001**, *105*, 7602.
(2) Kisch, H.; Lindner, W. *Chem. Unserer Zeit* **2001**, *35*, 250.
(3) Nozik, A. J.; Memming, R. *J. Phys. Chem.* **1996**, *100*, 13061.
(4) Kamat, P. V.; Meisel, D.; *Semiconductor Nanoclusters−Physical, Chemical,, Catalytic Aspects*; Elsevier: Amsterdam, 1997; Vol. 103.
(5) Licht, S.; Wang, B.; Mukerji, S.; Soga, T.; Umeno, M.; Tributsch, H. *Int. J. Hydrogen Energy* **2001**, *26*, 653.
(6) Schwarz, O.; van Loyen, D.; Jockusch, S.; Turro, N. J.; Duerr, H. *J. Photochem. Photobiol. A: Chem.* **2000**, *132*, 91.
(7) Oregan, B.; Grätzel, M. *Nature* **1991**, *353*, 6346.
(8) McConnell, R. D. *Renew. Sustain. Energy Rev.* **2002**, *6*, 273.
(9) Huang, S. Y.; Schlichthorl, G.; Nozik, A. J.; Gratzel, M.; Frank, A. J. *J. Phys. Chem. B* **1997**, *101*, 2576.
(10) Tachibana, Y.; Moser, J. E.; Grätzel, M.; Klug, D. R.; Durrant, J. R. *J. Phys. Chem. B* **1996**, *100*, 20056.
(11) Willig, F.; Zimmermann, C.; Ramakrishna, S.; Storck, W. *Electrochim. Acta* **2000**, *45*, 4565.
(12) Huber, R.; Spoerlein, S.; Moser, J. E.; Grätzel, M.; Wachtveitl, J. *J. Phys. Chem. B* **2000**, *104*, 8995.
(13) Asbury, J. B.; Hao, E. C.; Wang, Y. Q.; Ghosh, H. N.; Lian, T. Q. *J. Phys. Chem. B* **2001**, *105*, 4545.
(14) Huber, R.; Moser, J. E.; Grätzel, M.; Wachtveitl, J. *J. Phys. Chem. B* **2002**, *106*, 6494.
(15) Kelly, C. A.; Meyer, G. J. *Coord. Chem. Rev.* **2001**, *211*, 295.
(16) Hao, E.; Anderson, N. A.; Asbury, J. B.; Lian, T. *J. Phys. Chem. B* **2002**, *106*, 10191.
(17) Redfern, P. C.; Zapol, P.; Curtiss, L. A.; Rajh, T.; Thurnauer, M. C. *J. Phys. Chem. B* **2003**, *107*, 11419.
(18) Persson, P.; Lunell, S.; Ojamäe, L. *Int. J. Quantum Chem.* **2002**, *89*, 172.
(19) Vittadini, A.; Selloni, A.; Rotzinger, F. P.; Grätzel, M. *J. Phys. Chem. B* **2000**, *104*, 1300.
(20) Persson, P.; Lunell, S. *Sol. Energy Mater. Sol. Cells* **2000**, *63*, 139.
(21) Nazeeruddin, M. K.; Zakeeruddin, S. M.; Humphry-Baker, R.; Gorelsky, S. I.; Lever, A. B. P.; Grätzel, M. *Coord. Chem. Rev.* **2000**, *208*, 213.
(22) Srikanth, K.; Marathe, V. R.; Mishra, M. K. *Int. J. Quantum Chem.* **2002**, *89*, 534.
(23) Aiga, F.; Tada, T. *J. Mol. Struct.* **2003**, *658*, 25.
(24) Persson, P.; Lunell, S.; Ojamäe, L. *Chem. Phys. Lett.* **2002**, *364*, 469.
(25) Odelius, M.; Persson, P.; Lunell, S. *Surf. Sci.* **2003**, *529*, 47.
(26) Persson, P.; Bergström, R.; Lunell, S. *J. Phys. Chem. B* **2000**, *104*, 10348.
(27) Ramakrishna, S.; Willig, F. *J. Phys. Chem. B* **2000**, *104*, 68.
(28) Ramakrishna, S.; Willig, F.; May, V.; Knorr, A. *J. Phys. Chem. B* **2003**, *107*, 607.
(29) Rego, L. G. C.; Batista, V. S. *J. Am. Chem. Soc.* **2003**, *125*, 7989.
(30) Stier, W.; Prezhdo, O. V. *J. Phys. Chem. B* **2002**, *106*, 8047.
(31) Stier, W.; Prezhdo, O. V. *J. Mol. Struct. (THEOCHEM)* **2002**, *630*, 33.
(32) Stier, W.; Prezhdo, O. V. *Isr. J. Chem.* **2002**, *42*, 213.
(33) Stier, W.; Duncan, W. R.; Prezhdo, O. V. *Adv. Mater.* **2004**, *16*, 240.
(34) O'Regan, B.; Schwartz, D. T.; Zakeeruddin, S. M.; Grätzel, M. *Adv. Mater.* **2000**, *12*, 1263.
(35) Kruger, J.; Bach, U.; Grätzel, M. *Adv. Mater.* **2000**, *12*, 447.
(36) Huber, R.; Moser, J. E.; Grätzel, M.; Wachtveitl, J. *J. Phys. Chem. B* **2002**, *106*, 6494.
(37) Arango, A. C.; Johnson, L. R.; Bliznyuk, V. N.; Schlesinger, Z.; Carter, S. A.; Horhold, H. H. *Adv. Mater.* **2001**, *12*, 1689.
(38) Nogueira, A. F.; Durrant, J. R.; Paoli, M. A. D. *Adv. Mater.* **2001**, *13*, 826.
(39) Wang, Y.; Hang, K.; Anderson, N. A.; Lian, T. *J. Phys. Chem. B* **2003**, *107*, 9434.
(40) Szabo, A.; Ostlund, N. S.; *Modern Quantum Chemsitry*, 1st revised ed.; McGraw-Hill: New York, 1989.
(41) Casida, M. E.; Jamorski, C.; Casida, K. C.; Salahub, D. R. *J. Chem. Phys.* **1998**, *108*, 4439.
(42) Becke, A. D. *J. Chem. Phys.* **1993**, *98*, 5648.
(43) Perdew, J. P. In *Electronic Structure of Solids*; Ziesche, P., Eschrig, H., Eds.; Akademie Verlag: Berlin, 1991.
(44) Frisch, M. J.; Trucks, G. W.; Schlegel, H. B.; Scuseria, G. E.; Robb, M. A.; Cheeseman, J. R.; Zakrzewski, V. G.; Montgomery, J. J. A.; Stratmann, R. E.; Burant, J. C.; Dapprich, S.; Millam, J. M.; Daniels, A. D.; Kudin, K. N.; Strain, M. C.; Farkas, O.; Tomasi, J.; Barone, V.; Cossi, M.; Cammi, R.; Mennucci, B.; Pomelli, C.; Adamo, C.; Clifford, S.; Ochterski, J.; Petersson, G. A.; Ayala, P. Y.; Cui, Q.; Morokuma, K.; Malick, D. K.; Rabuck, A. D.; Raghavachari, K.; Foresman, J. B.; Cioslowski, J.; Ortiz, J. V.; Stefanov, B. B.; Liu, G.; Liashenko, A.; Piskorz, P.; Komaromi, I.; Gomperts, R.; Martin, R. L.; Fox, D. J.; Keith, T.; Al-Laham, M. A.; Peng, C. Y.; Nanayakkara, A.; Gonzalez, C.; Challacombe, M.; Gill, P. M. W.; Johnson, B.; Chen, W.; Wong, M. W.; Andres, J. L.; Gonzalez, C.; Head-Gordon, M.; Replogle, E. S.; Pople, J. A. *Gaussian 98*; Gaussian, Inc.: Pittsburgh, PA, 1998.
(45) Mukamel, S. *Nonlinear Optical Spectroscopy*; Oxford University Press: Great Britain, 1995.